Meta-Dynamic Recrystallization in the Ni-Based Superalloy Haynes 282

metals

MDPI

Article

Meta-Dynamic Recrystallization in the Ni-Based Superalloy Haynes 282

Emil Eriksson [1], Fabian Hanning [2], Joel Andersson [2] and Magnus Hörnqvist Colliander [1,*]

[1] Department of Physics, Chalmers University of Technology, SE-412 96 Göteborg, Sweden; emil.eriksson@chalmers.se
[2] Department of Engineering Science, University West, SE-461 32 Trollhättan, Sweden; fabian.hanning@hv.se (F.H.); joel.andersson@hv.se (J.A.)
* Correspondence: magnus.colliander@chalmers.se

Abstract: Forging on an industrial scale often involves slow, size-limited cooling rates or high temperature hold times between, or after, deformation. This enables the dynamic recrystallization (DRX) initiated during forging to further progress under static conditions, a phenomenon called meta-dynamic recrystallization (mDRX). As mDRX will influence the final grain size, and thus properties, it is critical to understand and control it during processing. Here, we study the mDRX evolution in Ni-based superalloy Haynes 282 during post-deformation hold times of up to 120 s at 1080 °C after partial DRX. We find that mDRX is the dominating mechanisms responsible for the microstructure evolution the hold time. The very rapid mDRX kinetics in the initial stages suggest that quench delays (the time between the end of the deformation and the onset of the quenching intended to arrest the microstructure evolution) must be kept well below 1 s in order to allow reliable conclusions to be drawn from post-deformation microstructure investigations. A larger prior strain (larger DRX fraction) leads to faster mDRX kinetics and a larger final grain size. Larger strains leads to earlier impingement of the growing grains, which, in combination with smaller remaining deformed regions into which the grains can grow, limits the maximum size of the mDRX grains. We also note a close correlation between static recovery and stress relaxation during the hold time, whereas no such correlation between mDRX and stress relaxation can be observed.

Keywords: Ni-based superalloys; meta-dynamic recrystallization; hot deformation; EBSD

Citation: Eriksson, E.; Hanning, F.; Andersson, J.; Hörnqvist Colliander, M. Meta-Dynamic Recrystallization in the Ni-Based Superalloy Haynes 282. *Metals* **2023**, *13*, 1335. https://doi.org/10.3390/met13081335

Academic Editor: Maciej Motyka

Received: 22 June 2023
Revised: 13 July 2023
Accepted: 20 July 2023
Published: 26 July 2023

1. Introduction

The mechanical properties of metallic materials are controlled by their microstructure, e.g., grain size and shape, texture, and presence of secondary particles. While the final properties of a component is typically determined by subsequent heat treatments, the starting microstructure originating from the prior thermomechanical processes defines the available property space. The term "thermomechanical" refers to the simultaneous application of plastic deformation and high temperature. This leads to synergistic effects where the stored energy from the plastic deformation drives microstructural changes, which in turn are enabled by the supplied thermal energy. The result is a range of dynamic processes, including dynamic recrystallization, DRX (either through discontinuous, dDRX, or continuous, cDRX, mechanisms) and dynamic recovery (DRV), which has been thoroughly reviewed in e.g., references [1,2]. Among these processes, DRX and subsequent grain growth have the largest effect on the property space as it defines the texture and the minimum attainable grain size during the following heat treatments. Therefore, understanding the microstructural evolution during the early manufacturing processes is critical for property optimization.

Furthermore, in the case of typical industrial components, the large size leads to relatively slow cooling rates (as quenching is often avoided due to the risk of cracking and deformation), or their complex shapes require multiple forging passes with intermittent

holding times. During such periods, partially recrystallized microstructures will continue to develop through so called post-dynamic recrystallization (pDRX) [2]. This term is sometimes used interchangeably with meta-dynamic recrystallization (mDRX), although the latter is a specific pDRX mechanism where grains previously nucleated during deformation can continue to grow after the deformation has stopped, gradually consuming the remaining deformed grains. Strictly speaking, pDRX occurs either through mDRX, static recrystallization (SRX), or a combination of the two. The difference between mDRX and SRX is that as the former depends on growth of existing grains/nuclei, it does not involve an incubation time. Consequently, mDRX is generally a very rapid process, leading to large changes in DRX fraction and grain size in very short times. SRX, on the other hand, involves a nucleation stage and is therefore associated with an incubation time, typically on the order of minutes [1–4]. The occurrence of pDRX (and the rapid mDRX process in particular) will therefore have a very large influence on the final microstructure after forging and thus the available property space of the final component.

The role of mDRX in the formation of the final microstructure is largest in alloys forged at high temperatures, such as Ni-based superalloys. These alloys are typically used in high temperature applications, such as hot sections of aircraft engines and turbine generators, due to high strength at elevated temperatures [5,6]. The good elevated temperature strength, however, leads to the need for very high forging temperatures, typically exceeding 1000 °C, where the mDRX process is extremely rapid [7]. However, in spite of its significant importance, mDRX in Ni-based superalloys (and austenitic heat resistant steels) have received comparatively little attention compared to DRX during deformation.

Many of the existing studies investigate the effect of interpass annealing times during multi-stage deformation (also called double-hit experiments) [8–19]. During such tests, a sample is deformed at high temperature to a pre-determined strain at which the deformation is stopped while the temperature is maintained. After a given interpass, annealing time load is applied again, and the "fractional softening" (the difference in the flow stress at the end of the first deformation and the yield stress during reloading) is measured. This fractional softening is then assumed to directly represent the recrystallized volume fraction. The benefit of this approach is that the effects of quench delays (which will be discussed later in more detail) are completely avoided. However, the direct correspondence between fractional softening and recrystallized fraction can be questioned, which will also be discussed in more details. Nevertheless, the results of these studies are in general agreement on the effect of the deformation process parameters: the mDRX process is accelerated by higher temperatures [8,10,11,13,14,17–19], higher strain rates [8,10,11,13,14,17–20], and larger degrees of deformation [10,13,15]. The accelerating effect of strain rate is often connected to the general increase in the dislocation density (stored energy), leading to a larger driving force for mDRX as well as the higher density of DRX nuceli. Another potential effect is the more pronounced adiabatic heating during faster deformation, which leads to temperatures higher than target and would therefore be an alternative manifestation of the temperature dependence [7]. This effect would also lead to a dependence on the applied heating method. The thermal inertia during heating in conventional radiation furnaces is too large to allow effective closed-loop temperature control, and the temperature will increase beyond the target temperature and accelerate mDRX. In the case of resistive or inductive heating, the response time is fast enough to compensate for adiabatic heating for all but the highest strain rates [21], thus reducing the effects at lower strain rates. Nevertheless, even at intermediate strain rates, the temperature control system in such experiments requires time to counteract the adiabatic heating and the effect will depend on the exact combination of strain rate, strain and control system response. Unfortunately, the sample temperature evolution during hot compression tests is rarely reported in the literature, which makes comparisons between studies difficult. Regarding the effects of prior strain, there are a number of deviating reports, where some studies found only a very weak dependence on prior strain [11,19], contrary to the strong influence seen in, e.g., [10,13,15].

Some authors also report a significant effect of prior grain size [17,22], whereas others noted only a weak grain-size dependence [19].

There are, however, also studies which focus on the microstructural evolution during mDRX by direct observation, typically through interrupted hot compression tests with subsequent hold times [3,7,11,23–28]. The results of these studies are again in general agreement with the double-hit results, although they tend to reveal more underlying details, including, e.g., evolution of recrystallized grain size, grain boundary character, and misorentation and twin density. Zourari et al. [26] determined that it is the recrystallized fraction at the end of the deformation, rather than the strain level, which determines the mDRX kinetics. This can, to a large degree, explain the discrepancies in the reported effects of prior strain, as the DRX process is relatively slow in the early stages and even significant differences in strain level can result in very similar recrystallized fractions (similar kinetics).

However, while direct microstructural observations from interrupted tests provide much more information about the mDRX process, it has the drawback that it is very sensitive to the quench delay (the time between the end of the deformation and the initiation of the water quench aimed at preserving the instantaneous structure). As the mDRX process is extremely fast in the initial stages, even short quench delays on the order of seconds can lead to significant changes in the recrystallized fraction [7,29]. Unfortunately, the quench delay is rarely measured and reported in the literature. Available reports range from as small as 0.2 s [30] to the range 1–3 s [3,7,27,28] and even up to 5–6 s [7].

In this study, we investigate the mDRX evolution after hot compression of Ni-based superalloy Haynes 282, a new γ' strengthened alloy with good fabricability and weldability due to its slow γ' precipitation kinetics [31]. Previously, Metzler et al. [24] investigated the microstructural evolution with annealing time for up to 2 h after deformation and showed that strain rate and prior strain only weakly influenced the final average grain size. In a previous study, we investigated the effect of temperature and strain rate on the final microstructure both after deformation and after a subsequent 90 s static hold at the deformation temperature [21]. We concluded that both temperature and strain rate have an effect on the DRX process, but after a 90 s, post-deformation hold mDRX had erased the effect of the strain rate and the final microstructure was mainly controlled by the temperature. Here, we investigate the mDRX process in Haynes 282 at a specific temperature (1080 °C) in more detail, focusing on the effect of prior strain on the kinetics. The specific temperature was chosen to be consistent with our previous studies [21,30,32]. Care was taken to maintain the quench delay to a minimum in order to reduce the effects on the measured kinetics.

2. Materials and Methods

Hot compression tests of Ni-based superalloy Haynes 282 (Haynes International Inc., Kokomo, IN, USA), with chemical composition as shown in Table 1,were performed on cylindrical samples 8 mm in diameter and 12 mm in length. Samples were machined from a 15-inch diameter billet and were extracted at a constant radial position in the billet to ensure similar initial microstructures. They were placed in a tube furnace (Carbolite STF15/75/450, Carbolite Gero Ltd., Hope Valley, UK) pre-heated to 1080 °C and annealed for 30 min in an Ar atmosphere in order to simulate the soaking used to achieve a homogeneous temperature before deformation in large-scale industrial forgings. After 30 min, the samples were water-quenched to prevent γ' precipitation [33]. Since the soaking was performed below the secondary carbide solvus temperature (1100 °C), small secondary carbides nucleated along grain boundaries. However, these do not have a significant effect on the recrystallization behavior, and their presence can be safely neglected [32].

The samples were then placed in a Gleeble 3800 (Dynamic Systems Inc, Poestenkill, NY, USA) thermo-mechanical simulator and heated to 1080 °C at a rate of 18 °C s^{-1} and compressed with a strain rate of 0.05 s^{-1} to different strains (0.2, 0.4 and 0.6) after temperature stabilization. As the temperature is higher than the γ' solvus of Haynes 282 [33], any precipitates formed during the heating will dissolve during the stabilization. Graphite discs were placed between sample and anvils in order to reduce friction. After complete

deformation, the samples were either directly water-quenched or held at the deformation temperature for varying times (5, 15, 60, and 120 s) before quenching. To allow accurate quantification of mDRX, it is critical to minimize the quench delay. For low strains, the mDRX contribution to the as-deformed microstructure (i.e., 0 s hold) could be substantial. With placement of the water nozzle as close to the sample as possible and pre-filling the hose between the water tank and sample chamber before compression, we reduced the quench delay to 0.2 s.

Table 1. Chemical composition of Haynes 282 (in wt.%) according to material certificate [21].

Ni	Cr	Co	Mo	Ti	Al	Fe	Mn	Si	C	B
bal	19.3	10.2	8.7	2.2	1.5	0.9	0.05	<0.05	0.06	0.004

After deformation, the samples were sectioned along the compression direction to expose the surface of the central volume of the sample. These cross-sections were ground using SiC papers with grits down to P4000 and ion-polished in a PECS Argon ion polishing system (GATAN Inc., Pleasanton, CA, USA) with an incident angle of 8° at an acceleration voltage of 6 kV for 90 min in order to remove the deformed material from the grinding and avoid potential artefacts from mechanical polishing. Electron backscatter diffraction (EBSD) analysis was performed in a GAIA Tescan (TESCAN, Brno, Czech Republic) focused ion beam-scanning electron microscope (FIB-SEM). A step size of 0.5 µm was used to map a total area of 500 × 500 µm for each sample. Each map was acquired in two different scans and stitched together using the CHANNEL 5 Map Stitcher software (v. 5.12, Oxford Instruments, Abingdon, UK) in order to minimize the loss of focus for the rather large differences in depth for the uppermost and lowermost sections given the 70° tilt of the sample. However, slight differences when manually repositioning the beam introduced artefacts into the stitched maps, so all analyses were performed on the individual submaps and added together.

3. Results and Discussion

3.1. Initial Structure

The initial microstructure after the 1080 °C soak is shown in Figure 1a. Large blocky primary MC carbides can be seen within some grains, and smaller secondary carbides are located at grain boundaries. Figure 1b shows grain size distribution of the initial microstructure. This data was acquired from an EBSD measurement of a 2.5 × 2.5 mm^2 area with a step size of 7 µm. From this data, the average diameter of the grains was measured to 107 µm.

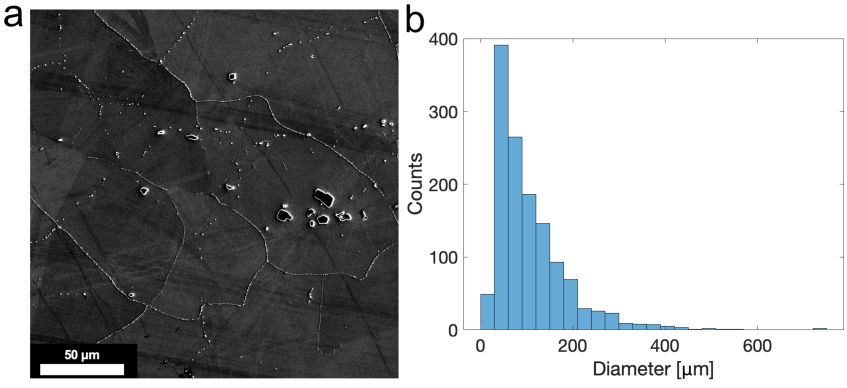

Figure 1. (**a**) Secondary electron image of the initial structure with a clear presence of both bulky intergranular primary carbides and smaller secondary located at grain boundaries. (**b**) Grain size distribution determined by EBSD.

3.2. Stress Response

Figure 2a shows the stress–strain curves for three samples deformed to different strains. In all cases, the strain is beyond the peak strain (ε_p, corresponding to the maximum in the stress–strain curve), and DRX should have initiated and progressed to different degrees [30]. The subsequent stress relaxation during the 120 s hold is shown in Figure 2b, where the vertical lines indicate the other investigated hold times: 5, 15, and 60 s. The stress–time data for shorter hold times are not shown, but the stress response closely matched the data obtained from the 120 s hold. As can be seen, the stress relaxation does not seem to be significantly affected by prior strain. The initial values at time 0 s are of course slightly different, but all samples show a very similar rate of relaxation down to about 50 MPa.

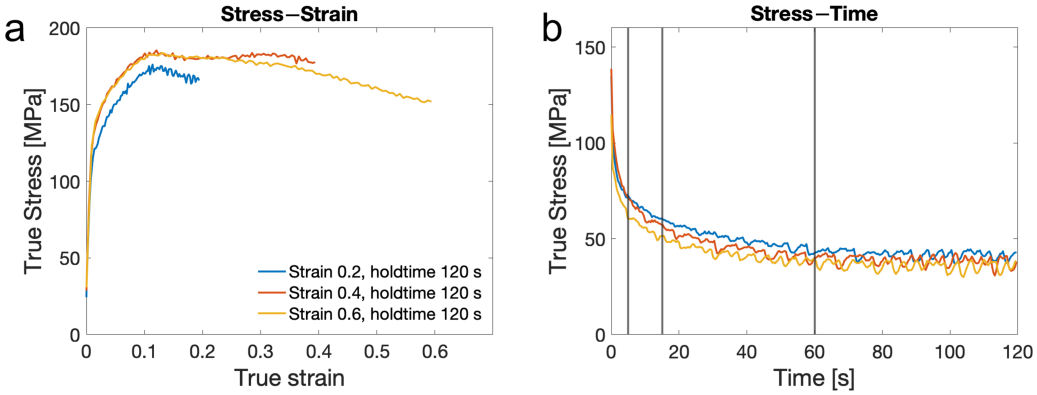

Figure 2. (**a**) Stress–strain curves and (**b**) stress–time curves for samples deformed to strains of 0.2, 0.4, and 0.6 and then held for 120 s. Vertical lines in (**b**) show the other investigated hold times: 5, 15, and 60 s.

3.3. Microstructure Evolution during Hold

Figure 3 shows the evolution of the microstructure during the hold time. Deformed grains are colored gray and recrystallized grains are shown in red. Classification was made based on the grain orientation spread (GOS) value of each grain. GOS is the average orientation difference between the pixels in a grain and the average orientation of the grain. A higher GOS value indicates a larger internal spread of orientaions in the grain, i.e., the presence of geometrically necessary dislocations (GNDs), indicative of plastic deformation. A threshold of 2° was used to separate deformed and recrystallized grains. During previous studies of the DRX process, we used a size threshold for classification, refs. [21,30,32] as this provided a more robust separation due to the large size difference between deformed and recrystallized grains in combination with the continuous evolution of internal misorientations during deformation [34]. However, mDRX involves the growth of already recrystallized grains, which at some point reach similar sizes as the remaining deformed regions. This leads to similar size distributions in the two classes (see, e.g., Figure 3h–j), and size-based classification fails. Furthermore, the absence of concurrent deformation during mDRX makes GOS-based classification more suitable.

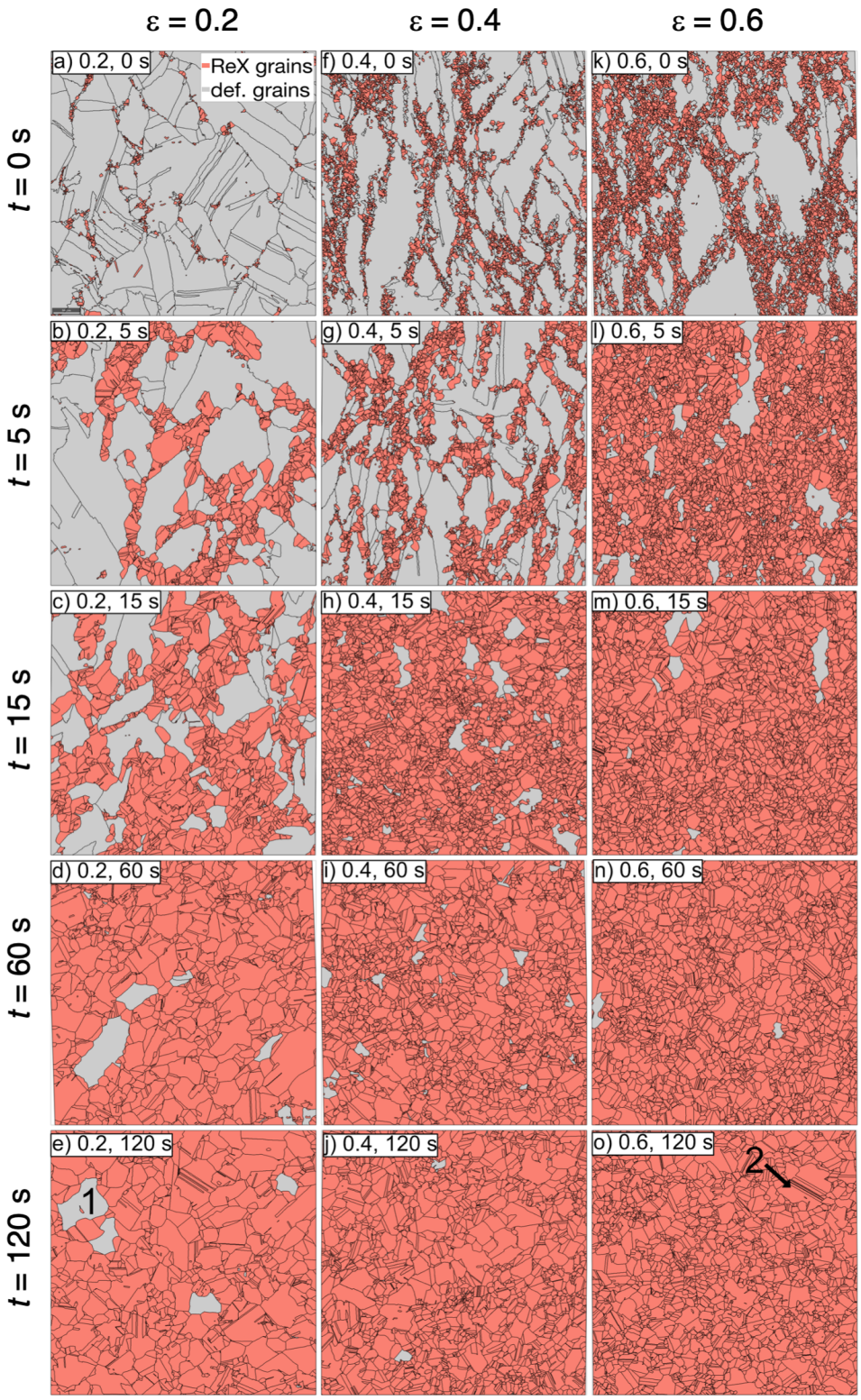

Figure 3. Maps showing deformed grains in gray and recrystallized in red for samples deformed to a strain 0.2 (**a**–**e**), 0.4 (**f**–**j**), and 0.6 (**k**–**o**) with hold time 0, 5, 15, 60, 120 s.

Nevertheless, manual correction of the classification was occasionally required. The highlighted grains in Figure 3e (marked as 1) and in Figure 3o (marked as 2) were both initially classified as deformed as their GOS values were larger than 2°. However, the spatial distribution of internal misorientations observed through the kernel average misorientation (KAM) maps of these two grains (Figure 4a,b) show that whereas grain 1 is clearly deformed,

with a pronounced dislocation substructure, grain 2 is actually, in principle, deformation-free, with the exception of a single low-angle boundary (LAB). This is further shown by the line profiles in Figure 4c,d, where (c) corresponds to the white line in Figure 4a,d and to the line in Figure 4b. As can be seen in Figure 4c, the accumulated misorientation in grain 1 increases progressively, indicating internal rotations of the lattice inside the grain even between the steps associated with individual LABs. For grain 2, on the other hand, the accumulated misorientation is close to zero until the 7° LAB is reached, then remains constant before returning to zero after the second boundary (Figure 4d). This indicates that with the exception of the single LAB, the grain is largely deformation-free. For the purpose of the present investigation, grain 2 was therefore re-classified as recrystallized. For each map in Figure 3, the corresponding KAM map was used to identify grains which had potentially been wrongly classified as deformed. Such grains were then manually inspected and, if necessary, reclassified as recrystallized.

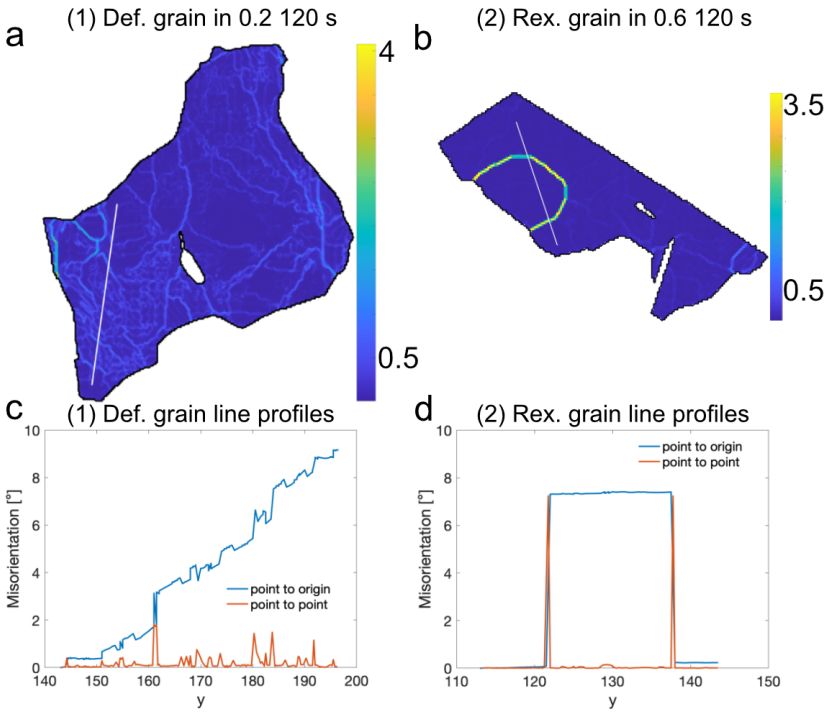

Figure 4. Differences in internal structure for two grains with GOS values larger than 2°. (**a**) KAM map for grain (1) in Figure 3e and (**b**) KAM map for grain (2) in Figure 3o. (**c**,**d**) are line profiles for lines shown in (**a**,**b**), respectively, where the blue lines show accumulated misorientation and the red lines shows point-to-point misorientations.

3.4. mDRX Kinetics

As can be seen in Figure 3a,f,k, DRX had indeed initiated already at the lowest strain (0.2) and progressed significantly at the larger strains (0.4 and 0.6). After a 5 s hold time (Figure 3b,g,l), the increase in the recrystallized fraction due to mDRX can be readily seen. The recrystallized fraction continues to increase with hold time at an apparently decreasing rate. The mDRX rate increases with prior strains. Only the sample deformed to a strain of 0.2 still had significant remnants of the original microstructure left after 120 s. The effect of the prior strain on the kinetics is further quantified in Figure 5. The total recrystallized fraction $X_{\mathrm{tot}}(t)$ (the sum of the DRX fraction after deformation, X_{DRX}, and the progressing mDRX consuming the remaining deformed regions) is shown in Figure 5a. The progression of mDRX with time is shown in Figure 5b in terms of $X_m(t)$, defined by the fraction of the remaining deformed regions which have deformed at time t according to Tang et al. [25]:

$$X_{\mathrm{tot}}(t) = X_{\mathrm{DRX}} + (1 - X_{\mathrm{DRX}})X_{\mathrm{m}}(t), \quad (1)$$

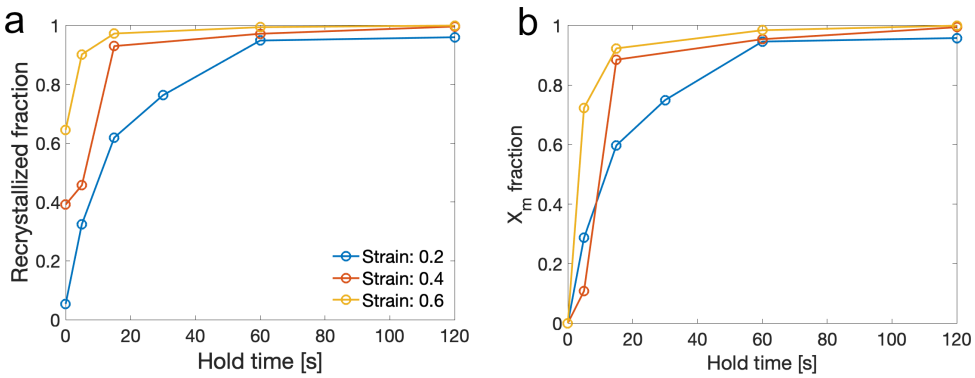

Figure 5. (**a**) Total recrystallized fraction and (**b**) mDRX fraction calculated with Equation (1).

As previously mentioned, X_{DRX} at time 0 increased with increasing applied strain, from approximately 0.05 at a strain of 0.2 to 0.25 at a strain of 0.4 and finally 0.65 at a strain of 0.6 (Figure 5a). Figure 5a,b also show the effect of prior strain on the mDRX rate. Note that one additional sample was held for 30 s after a strain of 0.2 in order to fully characterize the transient region. The time to (close to) full recrystallization decreases from around 60 s after deformation to a strain of 0.2, to 5 s after a strain of 0.6. This is due to the higher stored energy in the deformed grains at larger strains, which increases the driving force for mDRX (i.e., the lowering of the stored energy through consumption of deformed grains by growth of existing DRX grains) [7]. The extent of this effect can be expected to diminish at even larger strains, as dynamic recovery will lead to a steady-state situation at large strains. Furthermore, at least in the early stages, the larger number of nucleated DRX grains will lead to faster kinetics, as more grains can contribute to mDRX. However, the dominating mechanism in the current material is dDRX [21,30], which involves nucleation at grain boundaries. The limiting case is therefore expected to be when all previous grain boundaries contain DRX grains or nuclei. As mainly DRX grains in direct contact with deformed regions contribute to the consumption of the deformed microstructure, further increases in the number of DRX grains by nucleating more "layers" of grains/nuclei along the boundaries leads to a diminishing strain-induced acceleration. This is indeed seen in the present data. The acceleration of the mDRX process associated with an increase in the prior strain from 0.2 to 0.4 is much greater than the effect of an increase in prior strain from 0.4 to 0.6 (Figure 5a,b). This is presumably connected to the fact that the microstructure after a strain of 0.4 (Figure 3f) is very close to the limiting case, with all grain boundaries fully covered by DRX grains. After a strain of 0.6 (Figure 3k), most grain boundaries already contain multiple layers of DRX grains, but only the layer in direct contact with a deformed grain provides a major contribution to the mDRX process.

We also note that, as previously concluded by Nicolay et al. [7], the extremely high mDRX rates in the initial stages clearly emphasize the need for quench delay minimization when quantifying the amount of DRX from interrupted hot compression tests. The quench delay is seldom reported but has typically been measure to around 2 s or longer [3,7,27,28]. For interpolation between the as-deformed and 5 s hold data in Figure 5a, mDRX during a 2 s hold would increase the measured DRX fraction from 0.05 to 0.2 for a strain of 0.2 and from 0.65 to 0.8 for a strain of 0.6. (Notably, the 5 s data point after a strain of 0.4 does not follow the general trend, which is likely due to a statistical effect resulting from inhomogeneity of the microstructure.)

3.5. Effects of Static Recovery

Interestingly, whereas the prior strain level has a pronounced effect on mDRX kinetics (Figure 5a,b), it does not affect the stress relaxation to any significant degree (Figure 2b). This suggests that the stress relaxation is not (or at least not exclusively) connected to the progressing recrystallization process. Instead, it could be hypothesized that the relaxation

is controlled by the yield stress of the harder component of the partially recrystallized "composite" structure—the deformed grains. The deformed grains are expected to undergo static recovery (SRV) during the hold time, which will decrease the GND density and thereby also the yield stress. To examine this we plot the evolution of the average KAM value (a quantity which is related to the GND density) in the deformed grains with hold time in Figure 6. Clearly, this agrees much better with the stress relaxation in Figure 2b, which supports the above hypothesis. This could potentially have implications for the interpretation of the fractional softening after interpass annealing in multistage deformation (double-hit) experiments, which is commonly interpreted in terms of mDRX (and not recovery). However, further experiments with reloading of the samples at different hold times would be required to quantify the effect of the recovery on the yield strength. Finally, we note that the progressing recovery would also gradually reduce the driving force for mDRX during the hold time. This will be more pronounced for samples deformed to lower strains, where the kinetics are slower and allow more time for recovery.

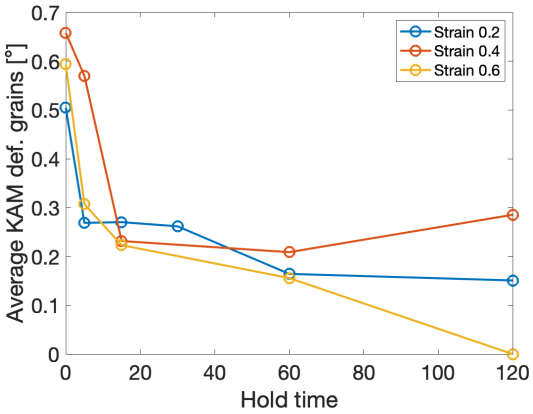

Figure 6. Average KAM of the remaining deformed grains in each sample.

3.6. Grain Size Evolution during mDRX

Figure 7 shows the evolution of the size (equivalent diameter calculated from the measured grain area) of the recrystallized grains with hold time. The sample deformed to a strain 0.2 shows a slightly smaller grain size after deformation, which is expected as the grain size will increase during DRX [30]. However, it undergoes the fastest increase and shows substantially larger final grain size after 120 s hold. As previously discussed, the lower number of DRX grains at a strain of 0.2 will allow all of them to rapidly grow into the large undeformed regions. Furthermore, at larger strain the growth will be more competitive, with grains impinging on each other and hindering further growth. The larger the prior strain, the smaller the remaining deformed regions will be, which limits the maximum size individual grains can reach. Also, the changing aspect ratio of the deformed grains with increasing strain will have a grain size limiting effect as impingement will happen earlier in grains with high aspect ratios due to the smaller shortest distance between grain boundaries from which the DRX grains grow. This effect is more clearly seen in Figure 8, where the entire grain size distributions are shown (with logarithmic probability scale to visualize the small number of large grains). After deformation to a strain of 0.2, the maximum grain size increases continuously with increasing hold time. After deformation to strains of 0.4 or 0.6, on the other hand, the grain size saturates already after 5–15 s hold time, after which it increases only slightly at longer times. From Figure 3, the above effects can be qualitatively seen through the significant inhomogeneity in the DRX grain size in the samples deformed to strains of 0.4 and 0.6, where large areas with smaller grains can be observed. These regions presumably correspond to areas with high densities of DRX grains after deformation, i.e., where limited growth has occurred, whereas the larger grains correspond to remaining deformed regions consumed by mDRX. Such effects could be partially responsible for the grain-size dependence of the mDRX kinetics reported [17,22].

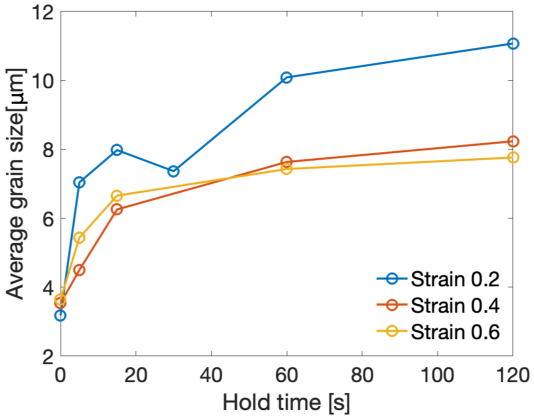

Figure 7. Average recrystallized grain size (in µm) for each strain and hold time.

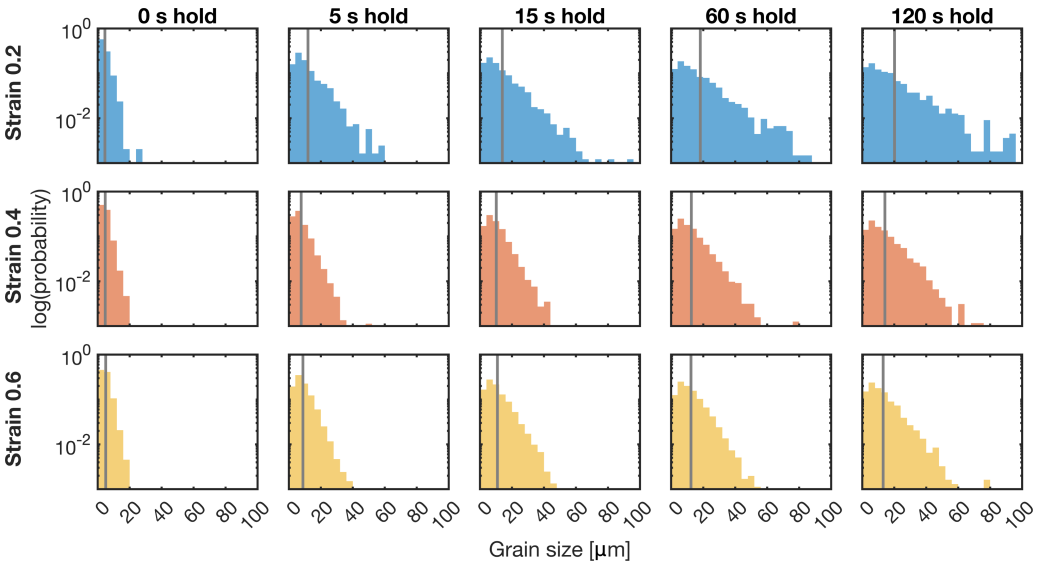

Figure 8. Grain size distribution histograms with logarithmic probability axis to visualize the small number of large grains. The gray lines are the average grain size in each histogram.

3.7. Number Density of Recrystallized Grains

As mDRX is assumed to proceed through growth of pre-existing DRX grains only, the number density of recrystallized grains should be constant until the recrystallization is complete and grain growth takes over. This is, however, not what can be observed from Figure 9, where the DRX grain number density (the number of grains classified as recrystallized, divided by the mapped area) is plotted as a function of hold time. After deformation to a strain of 0.2, the number density initially increases during the first 30 s. Nicolay et al. [7] suggested that pDRX at subsolvus temperatures in Alloy 718 mainly progressed through mDRX at higher strain rates, whereas the SRX contribution increased with decreasing strain rate below 0.01 s^{-1}. Qiao et al. [23] also reported the occurrence of SRX during pDRX for samples deformed to very small strains (0.1) where, in principle, no visible DRX had occurred. Using in situ EBSD studies of pDRX of Alloy 718, Zouari et al. [26] reported the emergence of new recrystallized grains (SRX) during post-deformation annealing of a sample deformed to a strain of 0.25 in parallel to mDRX through growth of pre-existing grains. The incubation time was, however, in the order of 30–60 s, and it is thus unlikely that SRX could make a significant contribution to the number density of DRX grains at times much shorter than this. Another potential explanation is the possibility that there are nuclei present at the grain boundaries which are too small to be captured in the (relatively low spatial resolution) EBSD mapping. As can be seen in Figure 3a–c, there is still a significant length of grain boundaries between deformed grains without any recrystallized grains

visible. As potentially undetected nuclei at these boundaries grow during mDRX, they will become detectable by EBSD and included in the set of DRX grains. This behavior is not seen in samples deformed to larger strains, where instead a relatively rapid decrease in the number density of DRX grains can be seen within the first 15 s. A decreasing number density can only be explained by a gradual disappearance of grains, presumably associated with competitive growth, or "cannibalization", within the DRX fraction. This could occur due to differences in stored energy between DRX grains, as grains which nucleated early would experience some degree of deformation during the continued compression, or simply due to capillary effects. In our previous study [30], we also observed significant differences in the substructure (stored energy) between different newly formed DRX grains with similar size, even at the early stages where post-nucleation deformation had not yet occurred. The effect seems to be larger at a strain of 0.6, which could be due to larger differences in stored energy between grains at larger strains and/or a larger size range of DRX grains as the early grains have had more time to grow.

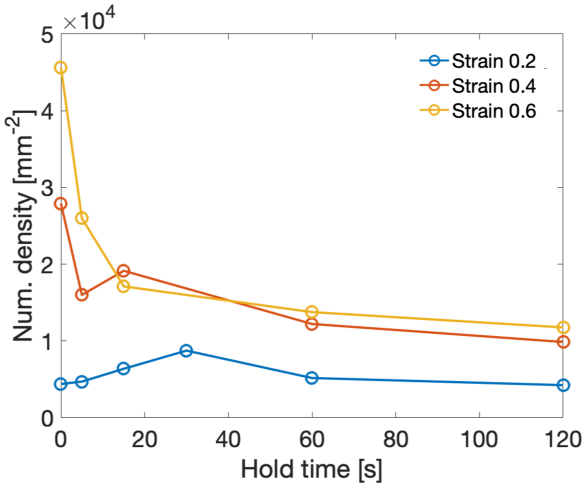

Figure 9. Number density for recrystallized grains.

4. Conclusions

The meta-dynamic recrystallization (mDRX) behavior of Ni-based superalloy Haynes 282 at 1080 °C after deformation to nominal strain levels between 0.2 and 0.6 has been investigated. The following conclusions can be drawn:

- The post-dynamic recrystallization (pDRX) is controlled by mDRX rather than static recrystallization (SRX), and the kinetics depend strongly on prior strain (DRX fraction), where larger strains lead to faster mDRX.
- The very rapid kinetics of mDRX will have significant impact on the measurements of DRX fractions from interrupted hot compression tests unless extensive care is taken to minimize the quench delay to times well below 1 s.
- The average size of recrystallized grains increases faster for lower strains, leading to larger final grain size. At larger strains the effect diminishes due to the earlier impingement of grains and the smaller deformed regions which can be consumed.
- In general, the number density of recrystallized grains decreases with time, initially at a very high rate which decreases at hold times above 15–30 s due to competitive growth. An exception to this is the behavior of the sample deformed to the lowest strain, where an increasing number density was observed at times below 30 s, followed by the same slow decrease as after larger strains. This was attributed to growth of pre-existing nuclei which were initially too small to be resolved by the EBSD but which grow to a detectable size during the early stages of mDRX.
- The stress relaxation during the hold time did not correlate with the evolution of the DRX fraction. Instead, it was found that static recovery controls the stress response,

which leads to questions regarding the validity of fractional softening during multi-step deformation experiments for characterization of mDRX.

Author Contributions: Conceptualization, methodology, validation, formal analysis, and visualization: E.E. and M.H.C.; investigation: E.E. and F.H.; resources: J.A. and M.H.C.; data curation and writing—original draft preparation: E.E.; writing—review and editing: E.E., F.H., J.A., and M.H.C.; supervision, project administration, and funding acquisition: M.H.C. All authors have read and agreed to the published version of the manuscript.

Funding: The funding for the present work has been provided by the Swedish Agency for Innovation (VINNOVA) through the Swedish National Aeronautical Research Program (NFFP) grant no. 2017-04863 in collaboration with GKN Aerospace Engine Systems AB.

Data Availability Statement: The data will be made available by the authors upon reasonable request.

Acknowledgments: This work was performed in part at the Chalmers Materials Analysis Laboratory, CMAL. Adrianna Lozinko at Chalmers University of Technology (Göteborg, Sweden) is acknowledged for her help with heat treatments.

Conflicts of Interest: The authors declare no conflicts of interest.

References

1. Huang, K.; Logé, R. A review of dynamic recrystallization phenomena in metallic materials. *Mater. Des.* **2016**, *111*, 548–574. [CrossRef]
2. Sakai, T.; Belyakov, A.; Kaibyshev, R.; Miura, H.; Jonas, J.J. Dynamic and post-dynamic recrystallization under hot, cold and severe plastic deformation conditions. *Prog. Mater. Sci.* **2014**, *60*, 130–207. .: 10.1016/j.pmatsci.2013.09.002. [CrossRef]
3. Zouari, M.; Bozzolo, N.; Loge, R.E. Mean field modelling of dynamic and post-dynamic recrystallization during hot deformation of Inconel 718 in the absence of delta phase particles. *Mater. Sci. Eng. A* **2016**, *655*, 408–424. [CrossRef]
4. Hatherly, M.; Rollett, A.; Humphreys, F.J.; Rohrer, G.S. *Recrystallization and Related Annealing Phenomena*; Elsevier Science & Technology: London, UK, 2004.
5. Donachie, M.J.; Donachie, S.; Donachie, M.J.; Donachie, S.J. *Superalloys : A Technical Guide*; A S M International: Materials Park, OH, USA, 2002.
6. Reed, R.C. *The Superalloys: Fundamentals and Applications*; Cambridge University Press: Cambridge, UK, 2006.
7. Nicolaÿ, A.; Fiorucci, G.; Franchet, J.; Cormier, J.; Bozzolo, N. Influence of strain rate on subsolvus dynamic and post-dynamic recrystallization kinetics of Inconel 718. *Acta Mater.* **2019**, *174*, 406–417. [CrossRef]
8. Cheng, Y.; Du, H.; Wei, Y.; Hou, L.; Liu, B. Metadynamic recrystallization behavior and workability characteristics of HR3C austenitic heat-resistant stainless steel with processing map. *J. Mater. Process. Technol.* **2016**, *235*, 134–142. [CrossRef]
9. Zhang, F.; Liu, D.; Yang, Y.; Liu, C.; Zhang, Z.; Wang, H.; Wang, J. Investigation on the meta-dynamic recrystallization behavior of Inconel 718 superalloy in the presence of δ phase through a modified cellular automaton model. *J. Alloys Compd.* **2020**, *817*, 152773. [CrossRef]
10. He, D.G.; Lin, Y.; Chen, M.S.; Li, L. Kinetics equations and microstructural evolution during metadynamic recrystallization in a nickel-based superalloy with δ phase. *J. Alloys Compd.* **2017**, *690*, 971–978. [CrossRef]
11. Gu, S.; Zhang, C.; Zhang, L.; Shen, W. Characteristics of metadynamic recrystallization of Nimonic 80A superalloy. *J. Mater. Res.* **2015**, *30*, 538–546. [CrossRef]
12. Liu, D.; Chen, J.; Chai, H.; Jiang, Y.; Li, Z.; Qiu, W.; Guo, Z. Study of meta-dynamic recrystallization behavior of GH5188 superalloy. *J. Mater. Res. Technol.* **2021**, *15*, 1179–1189. [CrossRef]
13. Zhang, C.; Zhang, L.; Shen, W.; Liu, C.; Xia, Y. The Kinetics of Metadynamic Recrystallization in a Ni-Cr-Mo-Based Superalloy Hastelloy C-276. *J. Mater. Eng. Perform.* **2016**, *25*, 545–552. [CrossRef]
14. Liu, J.; Liu, Y.; Lin, H.; Li, M. The metadynamic recrystallization in the two-stage isothermal compression of 300M steel. *Mater. Sci. Eng. A* **2013**, *565*, 126–131. [CrossRef]
15. Dehghan-Manshadi, A.; Barnett, M.; Hodgson, P. Recrystallization in AISI 304 austenitic stainless steel during and after hot deformation. *Mater. Sci. Eng. A* **2008**, *485*, 664–672. [CrossRef]
16. Sakai, T.; Ohashi, M.; Chiba, K.; Jonas, J. Recovery and recrystallization of polycrystalline nickel after hot working. *Acta Metall.* **1988**, *36*, 1781–1790. [CrossRef]
17. Na, Y.S.; Yeom, J.T.; Park, N.K.; Lee, J.Y. Simulation of microstructures for Alloy 718 blade forging using 3D FEM simulator. *J. Mater. Process. Technol.* **2003**, *141*, 337–342. [CrossRef]
18. Lin, Y.C.; Chen, X.M.; Chen, M.S.; Zhou, Y.; Wen, D.X.; He, D.G. A new method to predict the metadynamic recrystallization behavior in a typical nickel-based superalloy. *Appl. Phys. A* **2016**, *122*, 601. [CrossRef]
19. Chen, F.; Cui, Z.; Sui, D.; Fu, B. Recrystallization of 30Cr2Ni4MoV ultra-super-critical rotor steel during hot deformation. Part III: Metadynamic recrystallization. *Mater. Sci. Eng. A* **2012**, *540*, 46–54. [CrossRef]

20. Sun, W.P.; Hawbolt, E.B. Comparison between Static and Metadynamic Recrystallization. An Application to the Hot Rolling of Steels. *ISIJ Int.* **1997**, *37*, 1000–1009. [CrossRef]
21. Eriksson, E.; Hörnqvist Colliander, M. Dynamic and Post-Dynamic Recrystallization of Haynes 282 below the Secondary Carbide Solvus. *Metals* **2021**, *11*, 122. [CrossRef]
22. Lin, Y.; Wu, X.Y.; Chen, X.M.; Chen, J.; Wen, D.X.; Zhang, J.L.; Li, L.T. EBSD study of a hot deformed nickel-based superalloy. *J. Alloys Compd.* **2015**, *640*, 101–113. [CrossRef]
23. Qiao, S.; Wang, Y.; Lv, L.; Tan, G.; Cheng, T.; He, J. Post-dynamic recrystallization behavior of a powder metallurgy Ni-Co-Cr based superalloy under different deformation conditions. *J. Alloys Compd.* **2022**, *898*, 162961. [CrossRef]
24. Metzler, D.; Fahrmann, M.G. The Effect of Prior TMP on Annealed Grain Size in HAYNES 282 Alloy. In Proceedings of the 8th International Symposium on Superalloy 718 and Derivatives, Pittsburgh, PA, USA, 1 October–28 September 2014; John Wiley & Sons, Inc.: Hoboken, NJ, USA, 2014; pp. 379–389. [CrossRef]
25. Tang, X.; Wang, B.; Ji, H.; Fu, X.; Xiao, W. Behavior and modeling of microstructure evolution during metadynamic recrystallization of a Ni-based superalloy. *Mater. Sci. Eng. A* **2016**, *675*, 192–203. [CrossRef]
26. Zouari, M.; Logé, R.; Bozzolo, N. In Situ Characterization of Inconel 718 Post-Dynamic Recrystallization within a Scanning Electron Microscope. *Metals* **2017**, *7*, 476. [CrossRef]
27. Sharma, J.; Haghighat, M.H.; Gehrmann, B.; Moussa, C.; Bozzolo, N. Dynamic and Post-dynamic Recrystallization During Supersolvus Forging of the New Nickel-Based Superalloy—VDM Alloy 780. In *Superalloys 2020 Proceedings of the 14th International Symposium on Superalloys*, Virtual Event, 13–16 September 2021; Springer: Berlin/Heidelberg, Germany, 2020; pp. 450–460. [CrossRef]
28. Hafez Haghighat, M.; Sharma, J.; Gehrmann, B.; Alves, H.; Bozzolo, N. Supersolvus Recrystallization and Grain Growth Kinetics for the Fine Tuning of Grain Size in VDM Alloy 780 Forgings. *Metall. Mater. Trans. A* **2023**, *54*, 2092–2111. [CrossRef]
29. Guest, R.; Tin, S. The Dynamic and Metadynamic Recrystallisation of IN 718. In Proceedings of the Superalloys 718, 625, 706 and Various Derivatives, Pittsburgh, PA, USA, 2–5 October 2005; TMS: Warrendale, PA, USA, 2005; pp. 373–383. [CrossRef]
30. Eriksson, E.; Hanning, F.; Andersson, J.; Colliander, M.H. Dynamic recrystallization during hot compression of Ni-based superalloy Haynes 282. *J. Alloys Compd.* **2023**, *960*, 170837. [CrossRef]
31. Pike, L. Development of a Fabricable Gamma Prime Strengthened Superalloy. In Proceedings of the Superalloys 2008 (Eleventh International Symposium). TMS, Champion, PA, USA, 14–18 September 2008; pp. 191–200. [CrossRef]
32. Eriksson, E.; Andersson, J.; Hörnqvist Colliander, M. The Effect of Grain Boundary Carbides on Dynamic Recrystallization During Hot Compression of Ni-Based Superalloy Haynes 282. *Metall. Mater. Trans. A* **2021**, *53*, 29–38. [CrossRef]
33. Joseph, C.; Thuvander, M.; Persson, C.; Hörnqvist Colliander, M. Precipitation of γ' during cooling of nickel-base superalloy Haynes 282. *Philos. Mag. Lett.* **2021**, *101*, 30–39. [CrossRef]
34. Eriksson, E. Dynamic and meta-dynamic recrystallization of Ni-based superalloy Haynes 282. Ph.D. Thesis, Chalmers University of Technology, Gothenburg, Sweden, 2022.